GENERAL ELECTRIC

Research Laboratory

Quarterly Progress Report Number 23

MICROWAVE RESEARCH

Under Navy Contract NObsr-42463

Report No. RL-1117

31 May 1954

SCHENECTADY, NEW YORK

GENERAL ELECTRIC

Research Laboratory

Quarterly Progress Report Number 23

MICROWAVE RESEARCH

1 February - 30 April 1954

RL-1117

Prepared by

E. D. McArthur

for

U. S. Navy

Under Navy Contract NObsr-42463

G-E Requisition
EDG-35032

Approved by

James L. Lawson

Schenectady, New York
31 May 1954

FOR USE OF G-E EMPLOYEES ONLY

GENERAL ELECTRIC

Research Laboratory

SCHENECTADY, NEW YORK

TECHNICAL INFORMATION SERIES

Title Page

AUTHOR	SUBJECT CLASSIFICATION	NO.
McArthur, E. D.	microwaves--research and development	RL-1117
		DATE 31 May 1954

TITLE

MICROWAVE RESEARCH 42-702
Quarterly Progress Report Number 23

ABSTRACT

G.E. CLASS	REPRODUCIBLE COPY FILED AT	NO. PAGES
1	Research Information Services Section, The Knolls, Schenectady, New York	34
GOV. CLASS.		

CONCLUSIONS

By cutting out this rectangle and folding on the center line, the above information can be fitted into a standard card file.

INFORMATION PREPARED FOR U. S. Navy under Contract NObsr-42463

TESTS MADE BY

COUNTERSIGNED DIV.

DIVISIONS LOCATION

FN-610-1M-RL (2-50)

Foreword

During the quarter covered by this report, the amount of contractual support for this research program has been decreased. All of the projects that have made up the program in the past are reported here, and progress on each is brought up to date. However, the projects on Scalloped-beam Amplification (Task I, Item B), Resonant Spiral Circuits (Task II, Item E), and Microwave Tube Construction Techniques (Task IV) have been removed from the program and will not appear in future quarterly reports.

MICROWAVE RESEARCH

Quarterly Progress Report Number 23

TASK I - SMALL-SIGNAL MICROWAVE AMPLIFIER PRINCIPLES

A. Low-noise Triode Research - J. E. Beggs and N. T. Lavoo

The objective of this work is to learn the factors controlling the noise figure that may be achieved at frequencies above 1200 Mc in ordinary triodes suitable for receiver preamplifiers.

Work of this kind during the past several years has led to tubes like the GL-6299, which is now being produced and made available for general use.

Generally speaking, an advance in the art requires detailed improvements in tube-construction techniques, leading to the attainment of closer and more accurately controlled electrode spacings, improved electron emission, and better exhaust.

The experimental tubes in which these factors are being studied are designated numbers L-54 and L-55.

Ceramic insulators suitable for the assembly of L-54 and L-55 triodes have been received. Several diodes made from various groups of these parts have been operated on life test. The results of these tests are tabulated below.

Tube No.	Heater Voltage (volts)	Heater Current (amps)	Heater Power (watts)	Plate Current (ma)	Life (hours)	Failure
K-1	5.5	0.077	0.423	10	311	Open heater
K-3	8.0	0.080	0.640	10	399	Slow leaker
K-4	6.7	0.050	0.335	10	351	Low emission
N-1	1.0	0.425	0.425	15	166	Low emission
V-2	1.0	0.410	0.410	10	1161	Emission started to decline
K-58	52	4 ma	0.208	10	174	Open heater

Tube No. V-2 was made with ceramic parts that were vacuum-fired at approximately 1400°C. The characteristics of this diode were extremely stable for the first 900 hours of operation. Tubes Nos. K-4 and K-5 employed a more efficient heater design. All tubes had a cathode emitting area of approximately 1/60 cm^2, so that a plate current of 10 ma corresponds to a current density of 600 ma/cm^2.

Several of these tubes are of a quick-heating variety that requires less than three seconds to become operative. It is anticipated that heating times of less than one second are possible by reducing the mass of the cathode lid by a reasonable amount. It is rather encouraging that operation of 100 hours and more has been obtained with heater powers in the 1/4-watt range. This low power makes it possible to build cathodes having a high degree of thermal stability. This is of particular importance to the low-noise triode program, since it makes more practical the close spacing between cathode and grid proposed for the L-54 type.

Figure 1 shows the type of diode used to test these low-wattage heater-cathode units. The cathode is composed of a ceramic wafer having an oxide-coated metallic surface on one side and a resistive film which acts as the heater on the other side. This wafer is supported by a thin foil cylinder which serves as the cathode connection and one connection to the resistive film heater. A fine wire connected to the center of the resistive film provides the other heater connection.

Previously, the planar-type receiving-tube cathodes used had the heater inserted in a tube of metal extending downward from the cathode lid. This metal tube was useful in conducting heat to the lid. At the same time, however, it radiated considerable heat to the surrounding support cylinder. This increased the temperature of the support cylinder and consequently its elongation. Elimination of this inner metal tube by applying the heater directly to the back of the cathode lid thus improves both the heater efficiency and the cathode stability.

As a result of this work, it has been possible to build sample tubes that exhibit much more stable electron emission. The attainment of this stability has been a primary objective and is considered to be of fundamental importance to further progress in achieving lower-noise microwave triodes. Although the stability to be discussed in this report was obtained on diodes, the most recent work has resulted in triodes with good stability. However, the other characteristics of these triodes have not been measured in detail as yet.

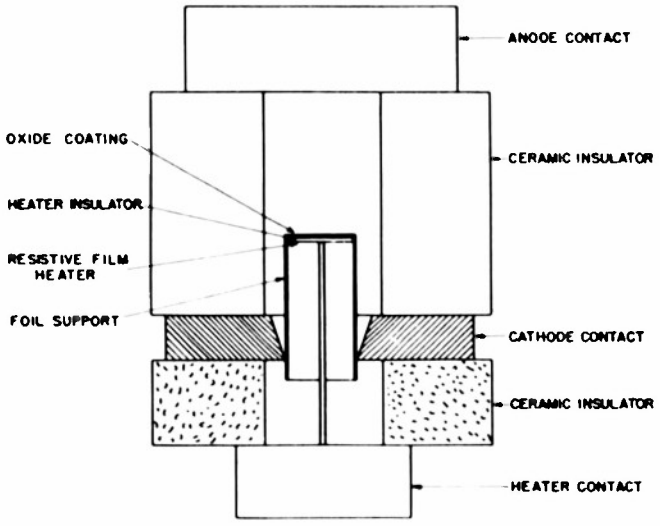

Fig. 1

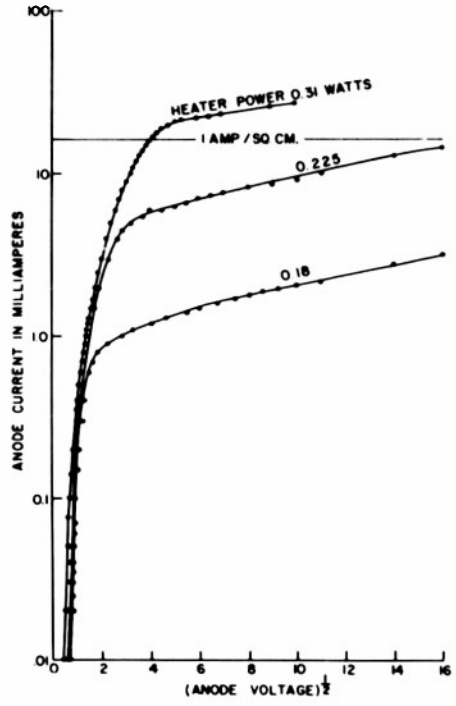

Fig. 2 Schottky plot, Diode A-5.

Figure 2 shows a Schottky-type saturation plot, which was taken on a diode with d-c voltages. The ability of the oxide cathode of this diode continuously to withstand the electric field necessary to take such a plot illustrates the unusual stability of the cathode.

Just what this stable emission means in terms of achieving improved low-noise microwave triodes can be explained in the following way. The fundamental limitations to obtaining lower-noise figures are the emitter temperature and cathode-to-grid transit time. Obtaining stable electron emission allows the temperature of the cathode to be dropped to allow only a minimum excess of available electrons necessary for good space-charge control. With the oxide emitter in a conventional tube, such operation is not possible except with greatly reduced life. Operation with a minimum of excess electrons is helpful in a number of ways. It reduces the numbers of electrons that go only part way out to the potential minimum, only to return back to the cathode. A reduction in this group should reduce the total emission damping. In addition,

increasing the ratio of operating current to available current reduces the depth of the potential minimum. This results in a higher average velocity of electrons crossing the potential minimum and substantially reduces the transit time. It is to be remembered that the reduction in the depth of the potential minimum is accompanied by the minimum shifting towards the cathode. This necessitates closer spacing of the electrodes, since the control element must be located at the potential minimum for maximum control. The maintenance of a maximum degree of space-charge control, even though there is only a minimum excess of available cathode current, is an important problem and is the next problem to be examined.

It is well known that, when low anode currents are drawn so that the potential minimum is beyond the anode of the diode under consideration, a conductance per milliampere of e/kT results. It is a further objective of this program to achieve as large a fraction of this value of e/kT as possible even though there be a large ratio of operating anode current to available current. Normally, in a diode, as the anode current is progressively increased by raising the anode voltage, the current is at first exponentially related to the voltage. This then gradually changes over to a region where the current is roughly related to the three-halves power of the voltage. This in turn is followed by a transition region where successive portions of the cathode surface become temperature-limited. The extent of this transition region will be determined by the uniformity of the electron emission, contact potential, and spacings. Finally, there follows a region where the anode current is insensitive to the anode voltage and there is current saturation. The latter regions are illustrated in a typical tungsten emitter diode in Fig. 3 for two values of heater voltage. The rather sharp break in the low-frequency dynamic conductance as temperature-limitation is approached is characteristic of the pure metal emitters. The transconductances of triodes of the L-31 type, which were previously built on this program, are illustrated in a similar type of plot in Fig. 4. Included are plots for two different types of emitters. Tube No. 51 has an oxide emitter, whereas No. 32 has an L-type cathode. The L-cathode tubes could be taken part way into the temperature-limited region with only slight deleterious effects on the emission, whereas this was not even attempted on a d-c basis on the oxide tube because of poisoning effects.

R-f tests of the oxide cathodes showed the best performance at currents near values at which the transconductance was breaking away from the normal transconductance - anode current characteristic. For instance, the best recorded noise figure of 10 db/kTΔf at 3000 Mc for oxide emitter No. 51 occurred at a heater voltage of four volts and an anode current of 14 milliamperes. Judging from the data of Fig. 4, this would place the operating point near the emission capability of the tube. It would not be anticipated that the tube life would be long

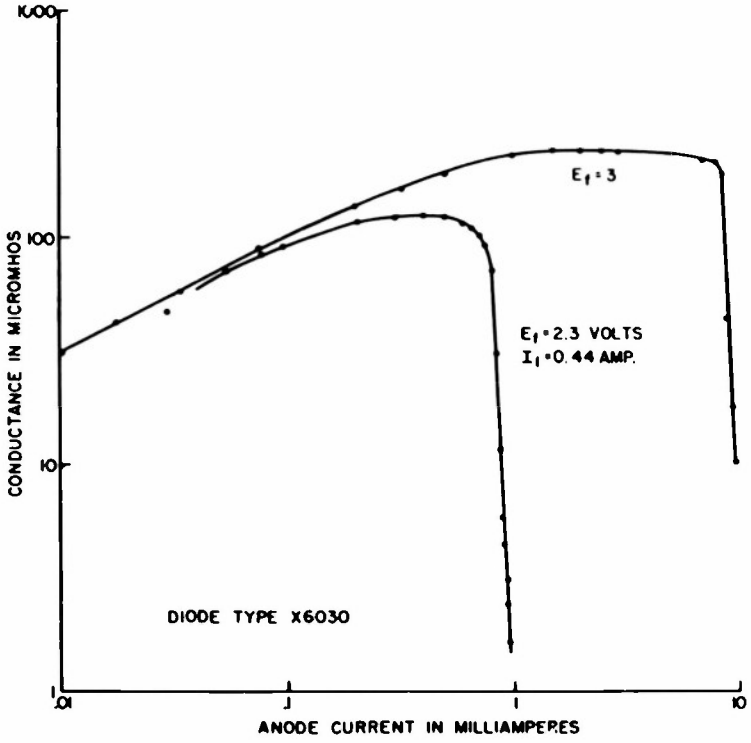

Fig. 3 Tungsten emitter conductance - anode current characteristic.

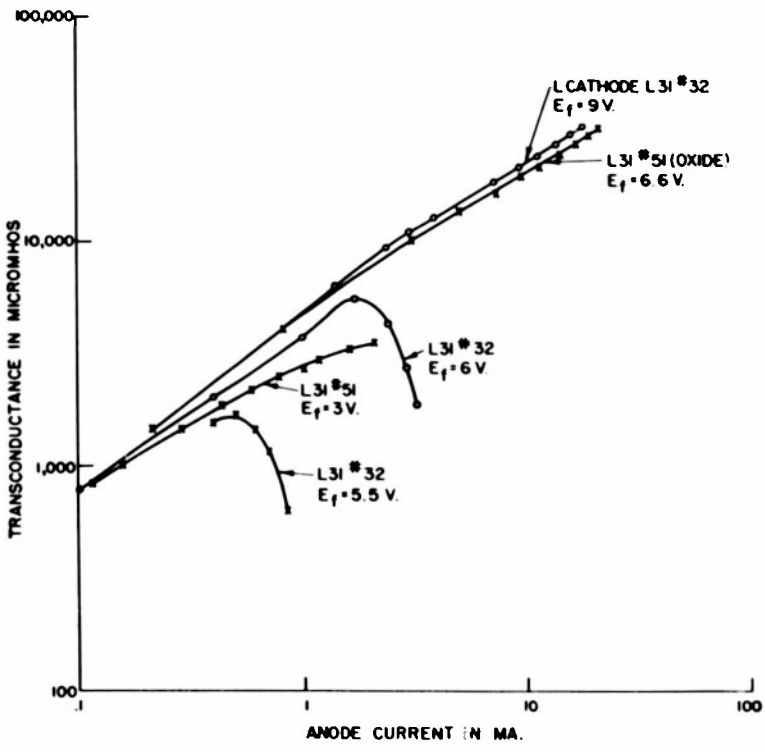

Fig. 4 Transconductance - anode current characteristics for the L-31.

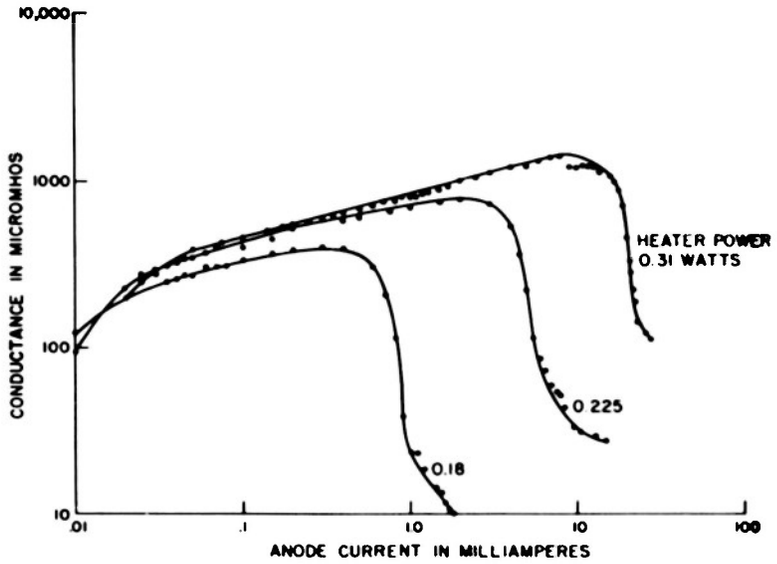

Fig. 5 Conductance - anode current characteristic, Diode A-5.

when it was operated in this manner because these early oxide-emitter tubes did not exhibit stability of emission at or near current saturation. On the other hand, although the L-cathode tube could be operated near current saturation with much more immunity, it was found that the r-f performance suffered considerably both in power gain and noise figure when operated anywhere near current saturation. Figure 5 illustrates the conductance - anode current plot of the diode whose Schottky plot was shown in Fig. 2. A fairly well-defined break in conductance is exhibited, although this is not so sharp as that of the tungsten emitter diode shown in Fig. 3. A point of inflection of the conductance curve is seen to occur at a value of anode current corresponding to the knee of the Schottky plot. The maximum of the conductance curve occurs at a current that gives a value of conductance per milliampere considerably below the e/kT value of approximately 11,600 micromhos per milliampere. This is partly explained by the rather wide (0.002 inch) spacing of this diode. In future work we hope to improve these characteristics and to achieve them on the more interesting triode.

The transit-time loading is one of the more important parameters in describing the microwave performance of a triode. As has been stated in a previous report, the L-54 shows promise of allowing a direct, accurate determination of this quantity. This past quarter, the techniques have been fairly well worked out for making a grounded-grid input conductance. A Smith chart presentation of these measurements is shown in Fig. 6. These

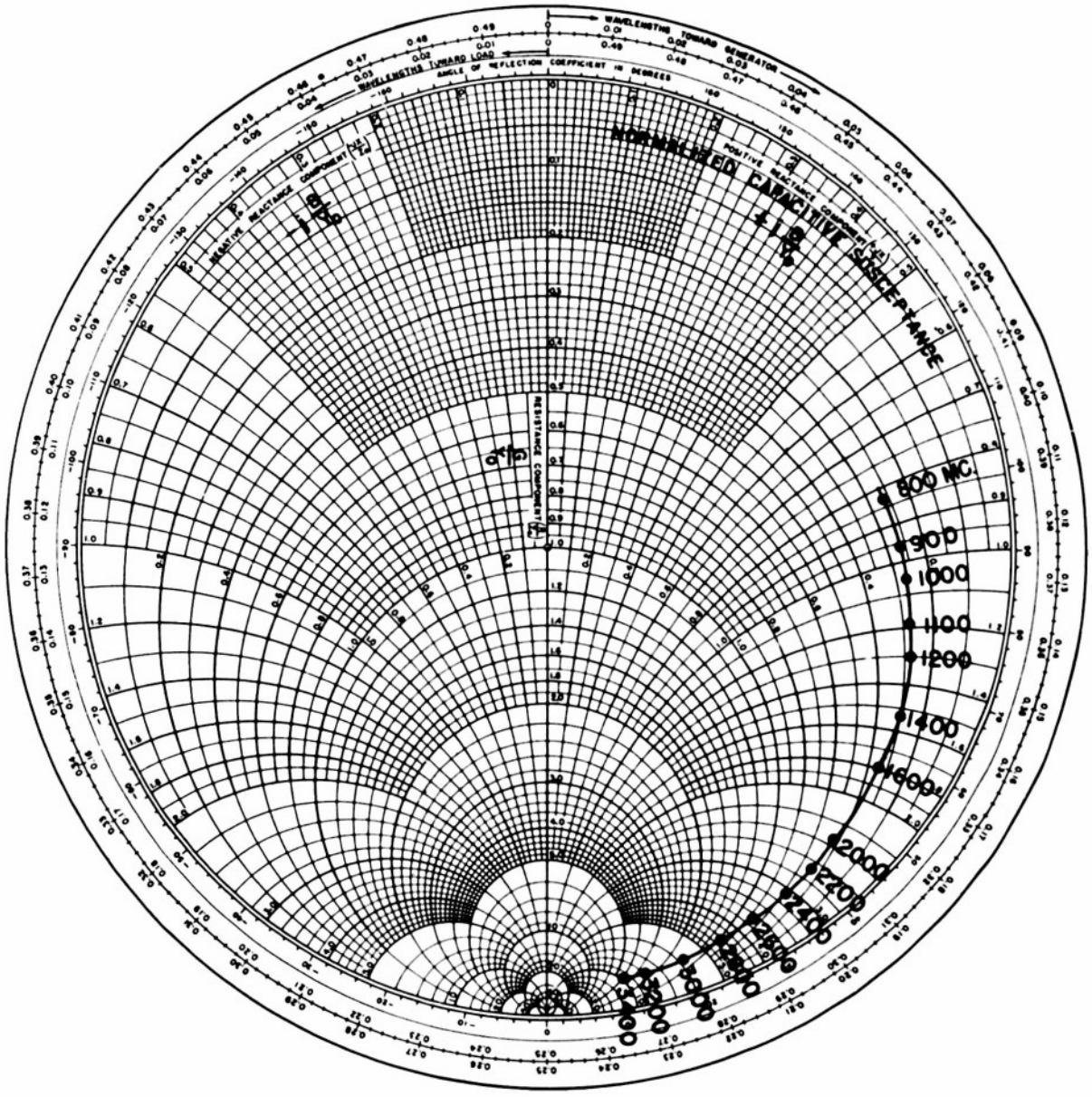

Fig. 6 L-54 input admittance at reference plane.

measurements were made on an early L-54 triode which was inserted with a minimum disturbance at the end of a slotted line whose characteristic impedance was 46.5 ohms. In this arrangement, the heater lead was brought through the hollow center conductor of the line. The measurements are tabulated with respect to a reference plane which is about 0.030 to 0.040 inch from the grid plane of the tube. It is this close proximity of the reference plane made possible by the unique construction of the L-54 that promises to make possible an accurate grounded-grid input-admittance measurement. On previous microwave tubes, because of the considerable separation between the reference plane and the electron stream, the accuracy of the admittance of the electron stream has been questionable. This is a result of the fact that the transforming network is such an important portion of the total admittance measured--a fact usually aggravated by the presence of an output resonance in the frequency range of interest. Because of the remoteness of the input resonance of the L-54, the initial computations on this tube have been made on the basis that a single series inductance was sufficiently accurate to transform admittance from the reference plane to the electron stream. The value of this inductance has been found to be 0.42 millimicrohenry for the L-54 measured. This value will vary somewhat from tube to tube because of the variation in the thickness of the cathode-grid ceramic. A plot of the apparent cold capacitance versus frequency as measured at the reference plane is sufficient experimental information for determining this series inductance. Such data (crosses) are shown in Fig. 7. By taking the values of the apparent capacitance at two frequencies (say, at 0.5 and 3 kMc), a two-element network consisting of the series inductance and the cold tube capacitance may be derived. Whether the single series-inductive element is sufficient may be judged by comparing the computed values of apparent cold capacitance versus frequency (using the derived series inductance and cold capacitance) with the measured values. The computed apparent capacitance is shown as the lower curve in Fig. 7.

The input conductance at the electron stream, after correction for the series inductance, is also shown (circles) in Fig. 7. The low-frequency transconductance of this tube was 4000 micromhos. Since a somewhat higher value at low frequencies is indicated by the experimental input-conductance data of Fig. 7, an extra source of loading may be indicated. Our previous work on other microwave tubes has indicated considerable loading on occasions, owing to losses in the oxide coating. In future work, arrangements will be made to evaluate such loading. At such time, the experimental data may fit a square-law variation better than the upper curve of Fig. 7. This curve has been computed by taking

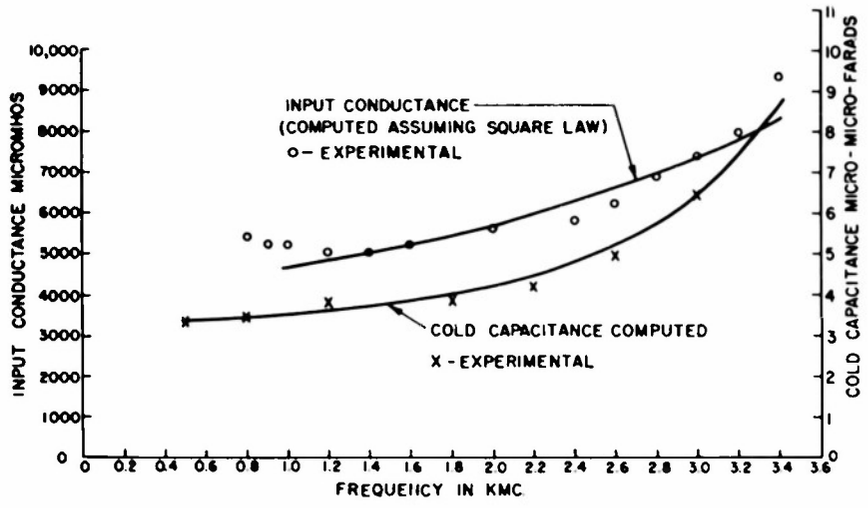

Fig. 7 L-54 input conductance at electron stream.

the measured input conductance at 1.4 and 3.0 kMc and assuming the total loading to consist of the transconductance (G_m) plus a term that varies as the square of the frequency. The resulting constants are:

$$G = G_m + G_t = G_m + K_f^2,$$

where $G_m = 0.00433$ mho,

$G_t = 0.00034\ f^2$,

f = kMc.

B. Scalloped-beam and Single-stream Amplification - T. G. Mihran

Scalloped-beam amplification is one of the three basic forms of space-charge-wave amplification. Its mechanism is understood physically and can be described mathematically. Excellent experimental verification of this phenomenon has been presented in previous progress reports. However, the occurrence of gain without apparent scalloping, as noted in Quarterly Progress Report No. 22, suggests that a second gain mechanism might be present. It is important to study both gain effects carefully in an effort to determine whether they are unique phenomena or merely different aspects of a more basic gain mechanism. It was toward this end that work this quarter was directed.

To obtain further verification of scalloped-beam amplification, the effect of the phasing between the scallops and the standing wave of current was studied. It was found that a reduction of the magnetic field strength causes an increase in both scallop wavelength and plasma wavelength. However, scallop wavelength increases faster than plasma wavelength, so the phasing is effectively altered. Output was studied as a function of magnetic field, with a fixed beam voltage of 500 volts and a cathode current of 50 ma. This case gives over 10 db of scalloped-beam gain with a magnetic field current of 0.295 amp. This corresponds to a magnetic field strength of 92 gauss (see Fig. 1 of Quarterly Progress Report No. 22). When the field current is reduced to 0.237 amp, there is essentially no scalloped-beam gain. Output versus drift distance for this case is plotted in Fig. 8. The important point to notice is the relative phasing between the standing wave of current and the beam scallops. It is shifted 90° from the optimum gain phasing. Debunching no longer takes place in the dense region of the beam, and rebunching does not occur in the expanded region. Each process occurs in a region centered about the equilibrium beam size, and what is gained during the first half of each process is lost during the last half of the process; hence there is no over-all gain. This is in accordance with our physical and mathematical understanding of the phenomenon.

A more complete picture of the effect of phasing can be obtained from Fig. 9. Here the relative gains at successive output maxima are plotted versus magnetic field current. At $I_m = 0.295$ amp, the phasing is right for optimum gain. The gain at each maximum drops off as magnetic field is reduced, until at $I_m = 0.237$ amp there is essentially no gain. This is the case plotted in Fig. 8. A further reduction of magnetic field current to 0.215 amp results in successive loss at each maximum. This would undoubtedly correspond to the "loss" phasing shown in Fig. 8. Below this point, scallop and plasma wavelengths begin to differ so greatly that phasing becomes a function of drift distance and no further simple conclusions can be drawn.

Before leaving Fig. 8, it is interesting to note that, even though the phasing has been adjusted so that there is no gain of the maxima, the minima are rising at the rate of 3 db per scallop. An obvious reason for this rise could be smearing due to velocity spread in the beam. However, an alternate explanation could be as follows. In addition to the usual space-charge-wave, a growing wave of current is started at the beginning of the drift tube with a very large initial loss. This growing wave would be evident only at the nulls of the space-charge-wave, at which points its presence would cause the current at the nulls to increase steadily. The advantage of this theory over the smearing theory is that such a growing wave would eventually take over and give monotonically increasing gain without standing waves. This is exactly the type of behavior that is observed experimentally.

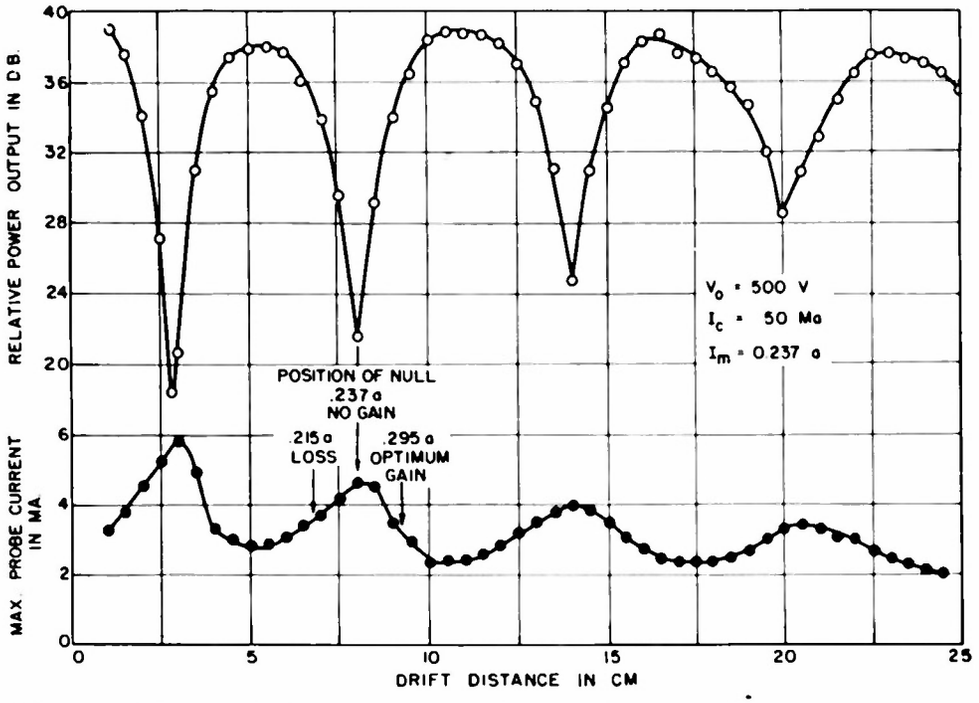

Fig. 8 Effect of phasing on scalloped-beam gain.

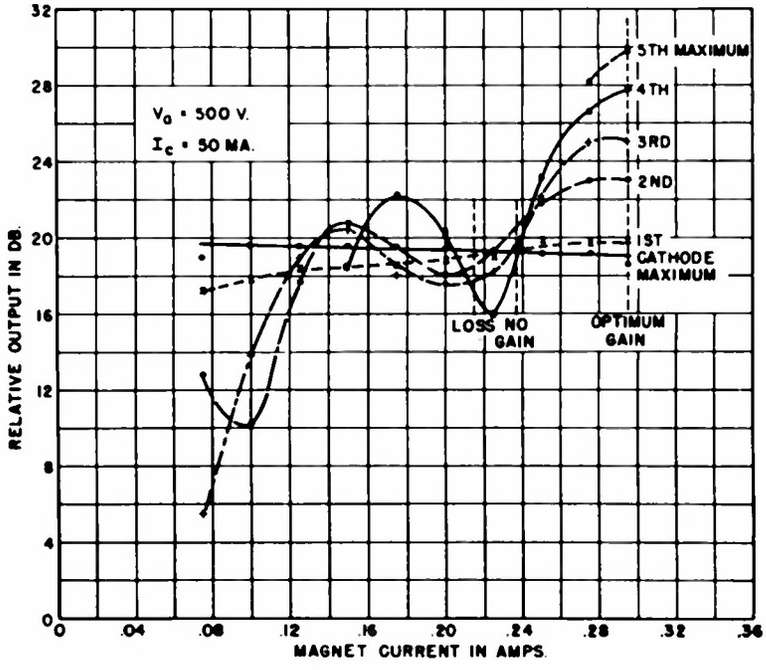

Fig. 9 Behavior of maxima with magnetic field.

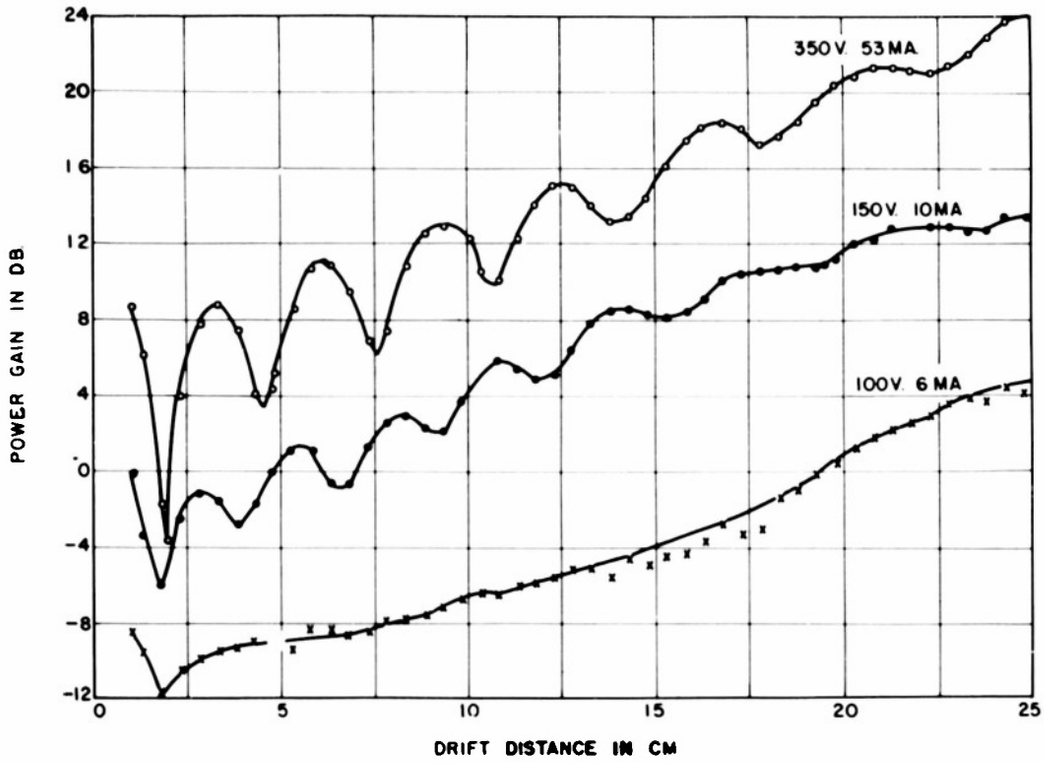

Fig. 10 Evolution from scalloped-beam amplification to anomalous gain.

In Fig. 10 several curves of output versus distance are plotted which show the gradual evolution from scalloped-beam amplification to anomalous gain. The lower curves were obtained by reducing the beam voltage, always adjusting cathode current for optimum gain at the end of the drift tube. The transit angle of the probe cavity is more than 200° for the lower curve, and this might account for some of the loss of resolution in going from the upper to the lower curves. However, this could not account for the loss of resolution along any single curve.

A final attempt was made to differentiate between the gain mechanisms by studying the dependence of gain upon gas pressure. Two such curves are shown in Fig. 11. The solid line shows the pressure-dependence of ordinary scalloped-beam amplification. Starting at a pressure of 2.8×10^{-6} mm, gain varies but little with pressure until 2×10^{-5} mm is reached. Gain then undergoes a 3-db rise as the pressure passes through 5×10^{-5} mm. Thereafter, gain drops quickly. The dashed

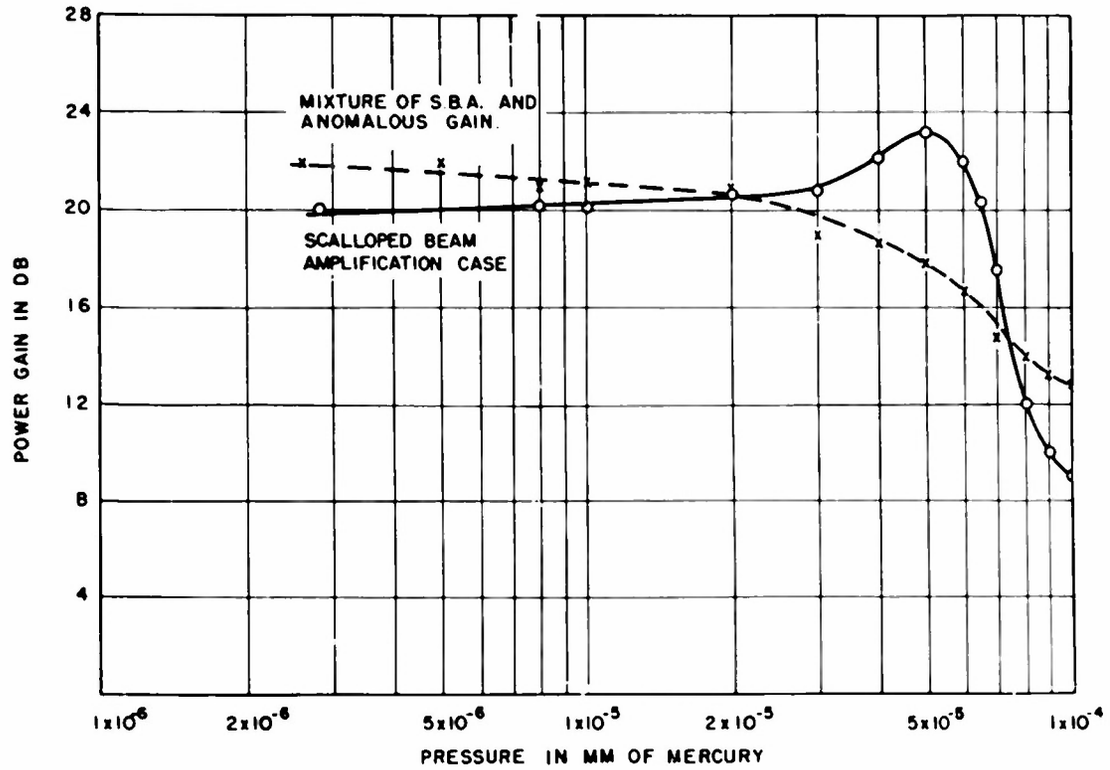

Fig. 11 Variation of gain with pressure.

curve is for a mixed case of scalloped-beam gain and anomalous gain. Gain in this case also varies only slightly as the pressure is increased to 2×10^{-5} mm; at higher pressures it drops steadily. From these curves, two conclusions may be drawn: (1) Neither type of gain is pressure-dependent in the usual pressure range for demountable tube operation (2×10^{-6} to 2×10^{-5} mm). (2) It seems probable that two different gain mechanisms are involved, since the pressure-dependence of the two curves differs. The hump in the solid curve is readily explained by the increase of collector current at higher pressures, owing to positive-ion focusing. This increase was actually observed experimentally.

No workable theory is yet in sight which will explain the anomalous gain. Future investigations will be designed to separate the two effects, if they can be separated. For the record, it should be noted that a gain of over 27 db due to the combination of effects has been observed recently, of which 17 db occurred in the drift space.

TASK II - TRAVELING-WAVE TUBES

A. A Wide-band Filter-type Traveling-wave Tube - M. R. Boyd

The design considerations and structural details of the periodically loaded traveling-wave tube have been previously covered in Quarterly Progress Reports Nos. 21 and 22. Since the work reported therein, much of the effort has been devoted to studying the operating characteristics of the tube.

The previously mentioned (Quarterly Progress Report No. 22) discrepancy between theoretical and measured values of $E^2/\beta^2{}_p$ has been resolved. Preliminary measurements of gain versus $(I_o/V_o)^{1/3}$ gave a value of five ohms at 800 Mc, whereas theoretical considerations and R/Q measurements indicated a value of 30 ohms. It has been learned that the slope method of measuring impedance is not reliable in structures having large values of the space-charge parameter Q. As $(I_o/V_o)^{1/3}$ is varied, QC will vary and A and B will change according to the theory of Pierce. Since B is assumed constant in computing impedance from the slope of the gain versus $(I_o/V_o)^{1/3}$ curve, this will give an erroneous answer for impedance.

A more suitable method for measuring impedance is that due to Kompfner.(1) The method consists of observing voltage and current at the point of cancellation of the three waves at the output end of the tube. Since a single measurement is made and QC will not change, the method is independent of space-charge variations and loss. Using the Kompfner method, the impedance at 800 Mc was found to be 28 ohms, which agrees with expectations.

It was also suspected that the apparent increase in impedance with increasing attenuator conductivity could be a result of the method of measurement. However, the phenomenon was still evident during impedance measurements by the different method. Fig. 12 illustrates the observed effect. To date, it has not been possible to obtain a net gain from the tube with a high-conductivity attenuator along the length of the tube, although the electronic gain is 50 or 60 db. The study of this resistive interaction is being continued at present. The tube will be sprayed with a low-resistance aquadag coating to provide a more symmetrical attenuator.

A series of low-level interaction measurements was made in order to examine the stability problems of the tube with respect to backward-wave oscillations. In Fig. 13, curves of frequency versus electronic phase shift at the maximum interaction voltage are shown for different values of beam perveance. Data taken with backward interactions are shown in dotted curves. From the

(1) Kompfner, R., "Operation of TWT at Low Level," J. Brit. Inst. Radio Eng., 10, 283 (1950).

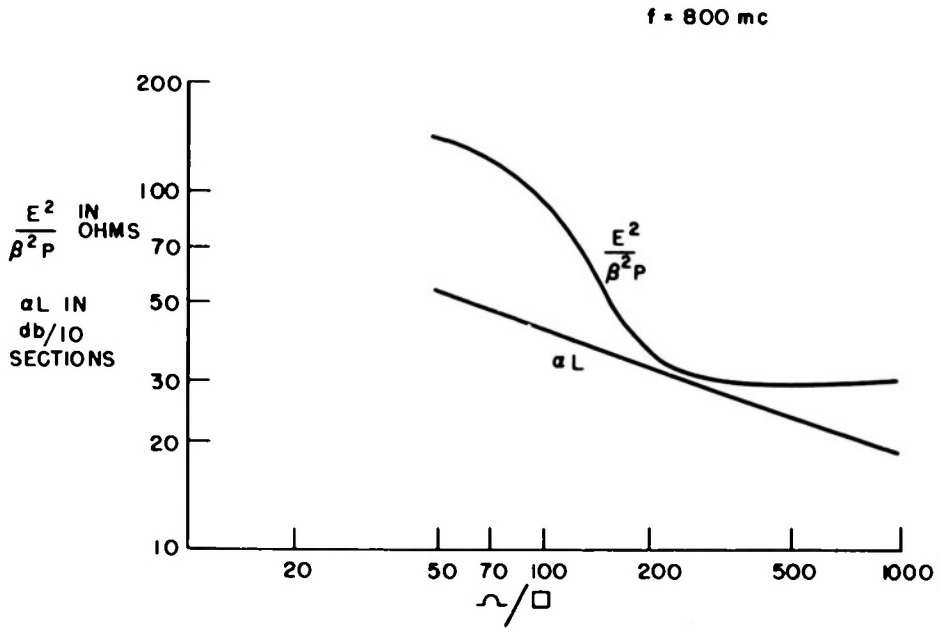

Fig. 12

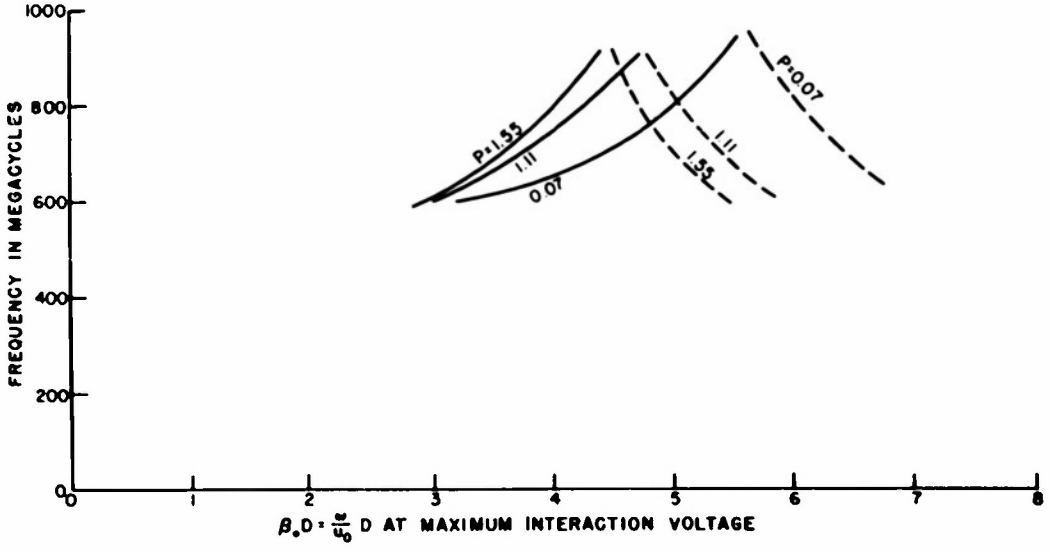

Fig. 13 Operating characteristics of filter TWT; tube uniformly attenuated (perveance in micropervs).

curves of Fig. 13, it would appear that interaction with a backward wave cannot be avoided and that the stability criterion is largely a matter of relative impedance or gain ratios at the operating frequency and corresponding backward-wave intersection. Although the data regarding the relative gain ratios are incomplete at present, it has been found that the interactions in the forward direction are 10 to 20 db higher. Furthermore, if the tube is allowed to oscillate, the oscillation frequency is in all cases at the low end of the frequency range and appears to be a forward oscillation which can be stabilized. It should be noted, however, that the stability to backward waves of a high-gain tube may present additional problems.

A longer tube having a nominal 20-db gain has been built, and a driver is being built to obtain saturation power measurements. With the present driver, 40 kilowatts at 23 per cent efficiency has been measured. More complete data on the high-level characteristics will be taken in the near future. Some preliminary work has been done on structure design for a tube at 7500 Mc.

B. Double-helix Traveling-wave Tubes - G. M. Branch

The double-helix tube No. DH-3, described in Quarterly Progress Report No. 22, has been disassembled and rebuilt with a different outer helix to constitute tube No. DH-4, as shown in Fig. 14. Because the glass envelope of the former tube was observed to have excessively loaded the outer helix, the pitch of the outer helix in No. DH-4 was increased by reducing the turns ratio from 4 TPI to 3-1/2 TPI in an attempt at compensation. The new ratio of $(\sqrt{k_b}\cot\psi_b)/(\sqrt{k_a}\cot\psi_a)$ has the value -1.06, close to the value -1.05, the theoretical optimum for cross-wound helices with no dielectric loading. (The terms k_b and k_a are the dielectric constants of equivalent uniform dielectric media having the same effect on the outer and inner helices as the glass envelope and support rods, and ψ_b and ψ_a are the pitch angles of the outer and inner helices, respectively.)

It is observed, however, that with this compensation the predicted propagation characteristics are not obtained. In Fig. 15 the theoretical propagation curves are shown as heavy curved lines. The relative phase velocities of the strongly interacting longitudinal mode, Mode 1, were obtained from observation of the synchronous voltage in the interaction between the circuit and a weak electron beam of two milliamperes. The observed data, indicated as circles, fall near the theoretical curve. The propagation characteristic curve of the transverse, weakly interacting Mode 2 was obtained as previously described from the resonance absorption peaks when the two helices were connected in parallel, and is seen to have a dispersion different from that expected for equivalent unloaded helices. One is led to conclude, therefore, that an alteration of pitch angle is not sufficient to compensate for unbalanced dielectric loading of cross-wound helices.

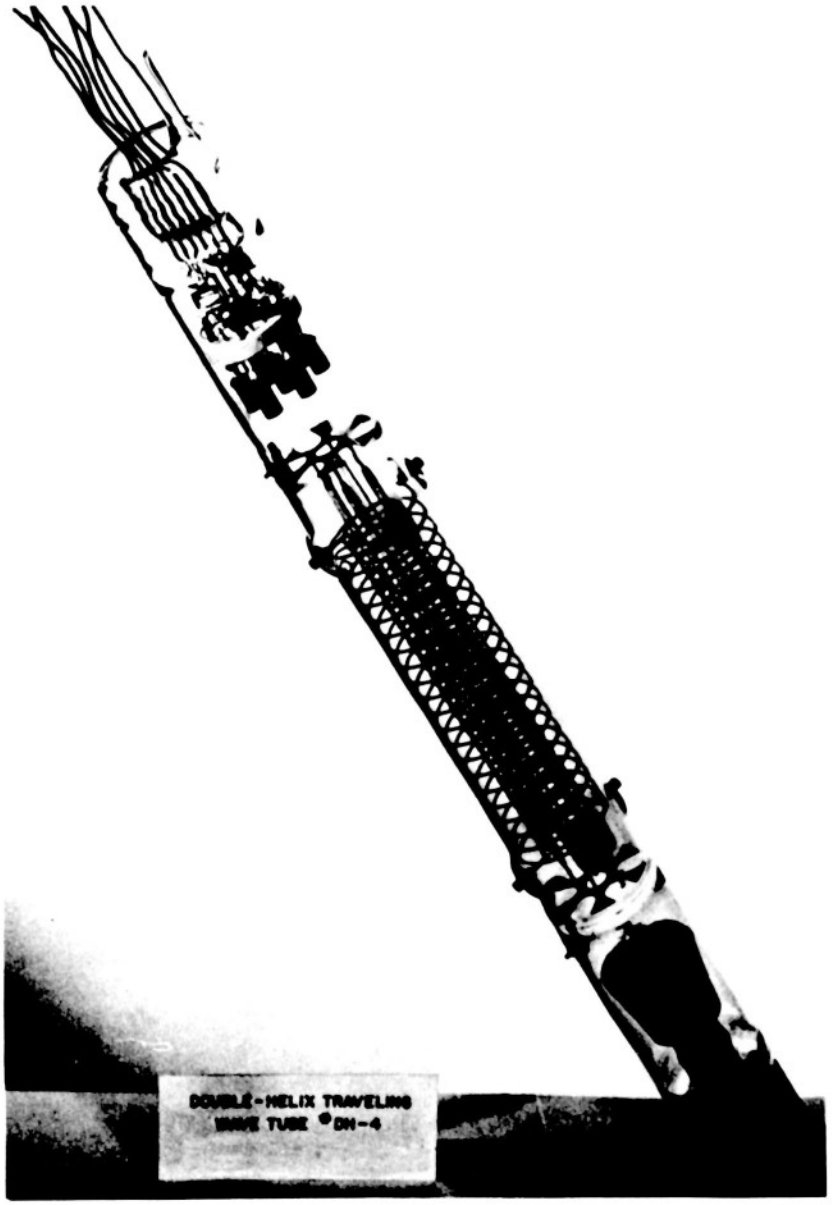

Fig. 14

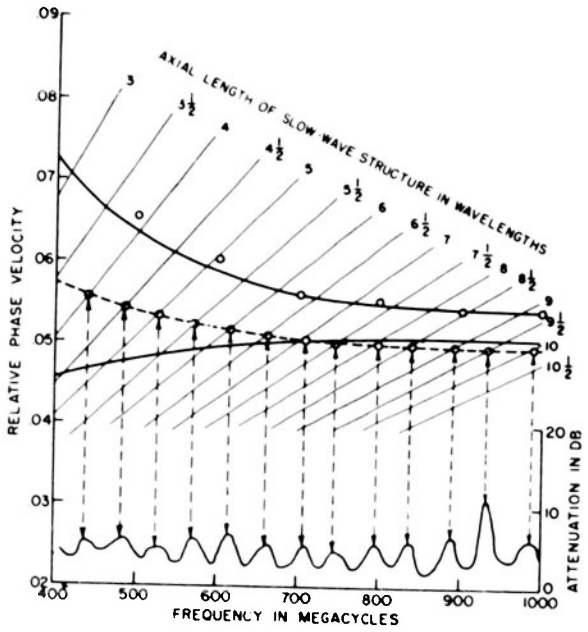
AXIAL LENGTH OF SLOW WAVE STRUCTURE IN WAVELENGTHS
3
3½
4
4½
5
5½
6
6½
7
7½
8
8½
9
9½
10
10½
RELATIVE PHASE VELOCITY
09
08
07
06
05
04
03
02
ATTENUATION IN DB
20
10
0
400
500
600
700
800
900
1000
FREQUENCY IN MEGACYCLES

Fig. 15

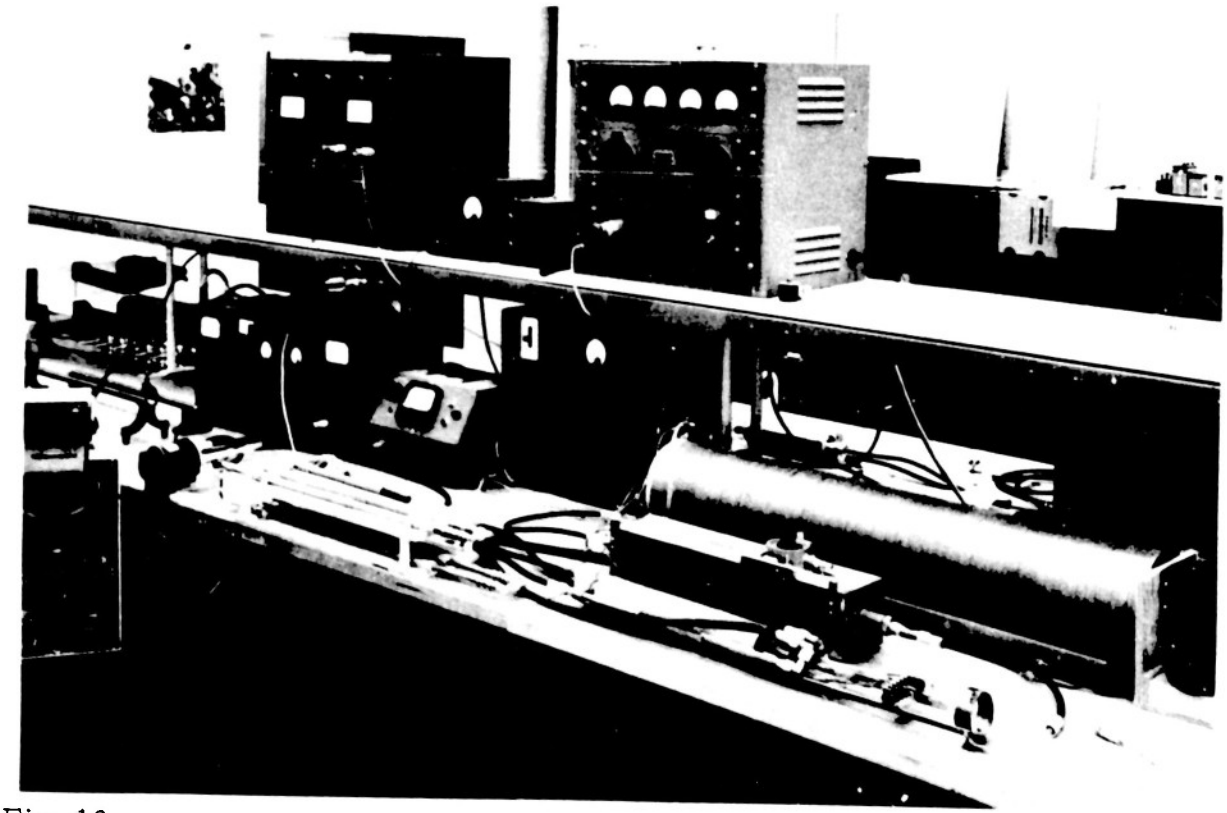

Fig. 16

The problem of mode excitation as a function of the relative phase of the input signals is being studied with this tube. As shown in Fig. 14, each helix has its input and output ends brought out through the envelope to individual terminations which may be connected to external coaxial circuits. Fig. 16 is a photograph of the circuits used to test the double-helix tube. On the overhead shelf are shown the filament, grid, and anode voltage supplies, and in the right background on the bench is the solenoid in which the tube is usually operated. A signal from the Boonton generator at the left on the bench is led through a tee to the two-decked trombone line stretchers in the middle foreground. With these two trombones, the length of coaxial line and hence the phase of the input signals can be varied independently to the two helix inputs. The tube is shown mounted in its four-terminal housing in the right foreground. The two input circuits were isolated with 10-db pads between the trombones and the tee and the outputs were led to separate matched loads or padded crystals.

The input - standing-wave ratios to both helices were measured simultaneously as the relative phase of the signal to the inner helix was advanced from zero to 360°. In addition, the relative amplitudes of the signals arriving at the separate loads on the two outputs were noted. Fig. 17 presents data taken at a signal wavelength of 39 cm for which the slow-wave structure is nonresonant in Mode 2. At the output end, Mode 2 is retarded 90° relative to Mode 1 because of the difference in propagation characteristics of the two modes. Fig. 18 presents data at 40 cm for which, according to Fig. 15, the slow-wave structure is 7-1/2 wavelengths long in Mode 2 and hence is resonant in this mode. In this case, also, Mode 2 is retarded about 90° with respect to Mode 1 at the output end. The variation of the input impedance as obtained from the position of standing-wave minima and the input VSWR when the two slotted lines are included in the input lines is sketched in Fig. 19.

The results shown in Figs. 17, 18, and 19 are in agreement with the theoretical expectation that Mode 1 is characterized by in-phase currents of about equal magnitude and Mode 2 by out-of-phase currents of about equal magnitude. The theoretical behavior of the two modes in the cross-wound helices is summarized in the vector charts of Figs. 20 and 21, which will now be compared with the experimental data of Figs. 17, 18, and 19.

The mode excitation and expected output currents for the non-resonant wavelength of 39 cm are shown in Fig. 20. The case of the resonant wavelength of 40 cm is treated in Fig. 21, in which an additional assumption is made that when the slow-wave structure is resonant in Mode 2, Mode 2 is excited in amplitude equal to Mode 1, even though for input lines

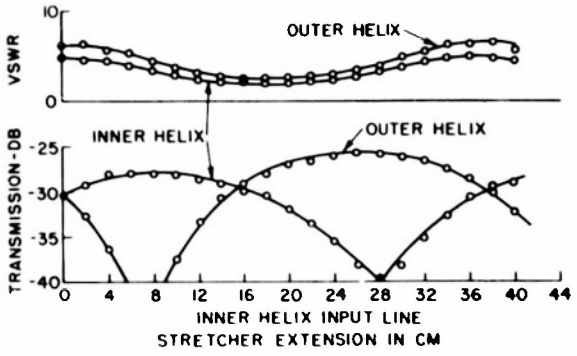

Fig. 17

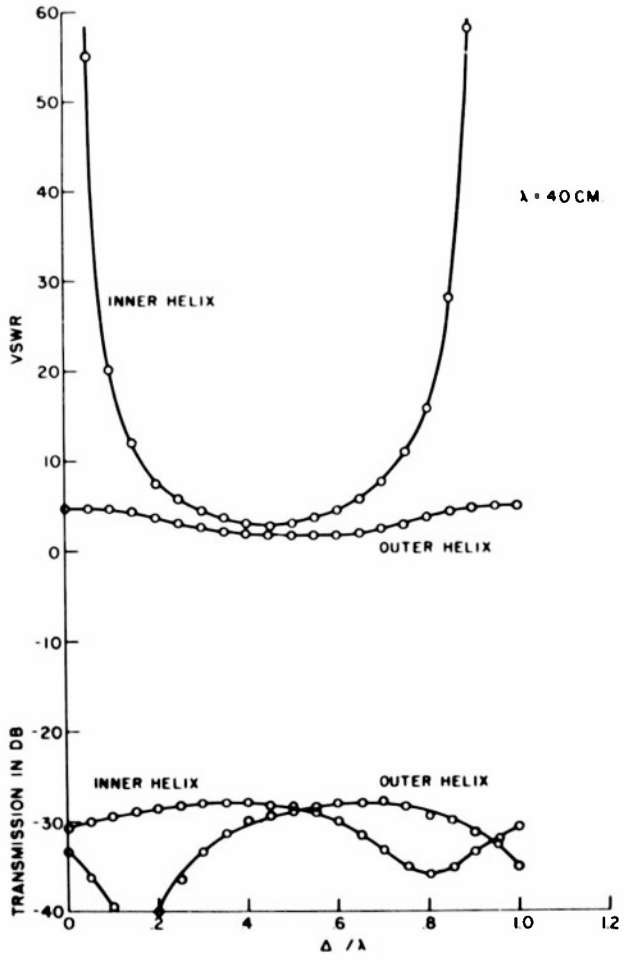

Fig. 18 Plot of transmission and input VSWR of TWT No. DH-4.

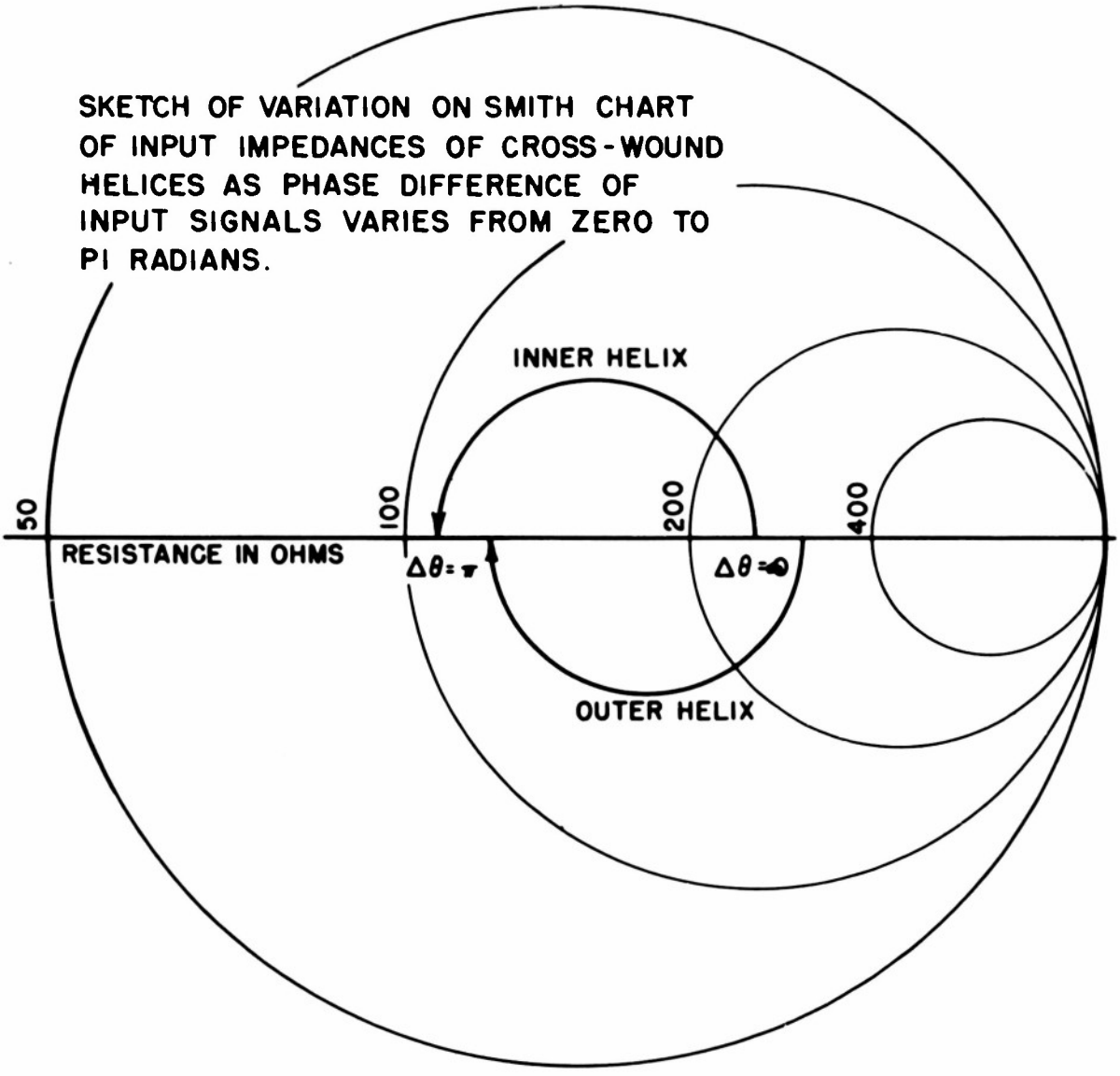
SKETCH OF VARIATION ON SMITH CHART
OF INPUT IMPEDANCES OF CROSS-WOUND
HELICES AS PHASE DIFFERENCE OF
INPUT SIGNALS VARIES FROM ZERO TO
PI RADIANS.
INNER HELIX
50
100
200
400
RESISTANCE IN OHMS
Δθ=π
Δθ=0
OUTER HELIX

Fig. 19

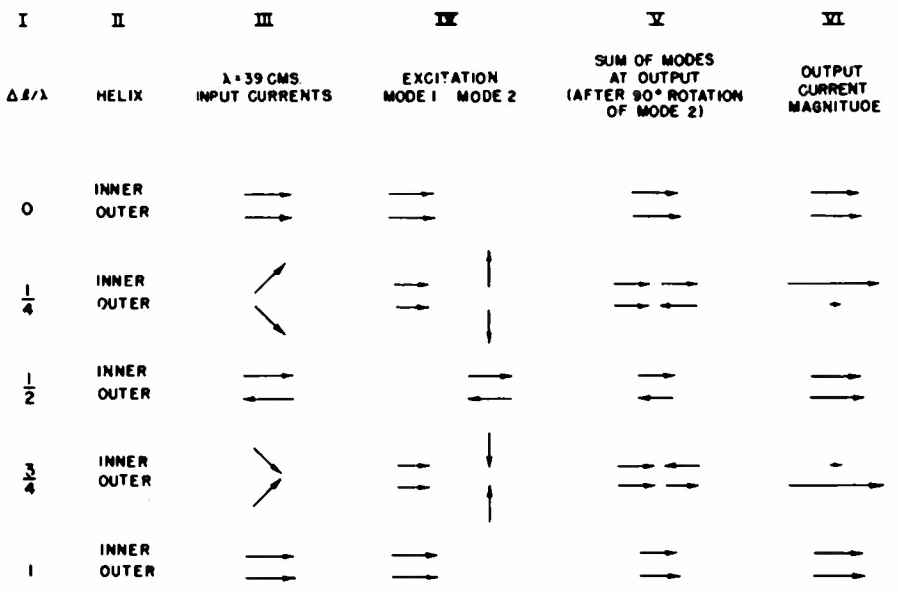

Fig. 20 Diagram of current vectors in cross-wound double helices (phases measured relative to current phase in Mode 1).

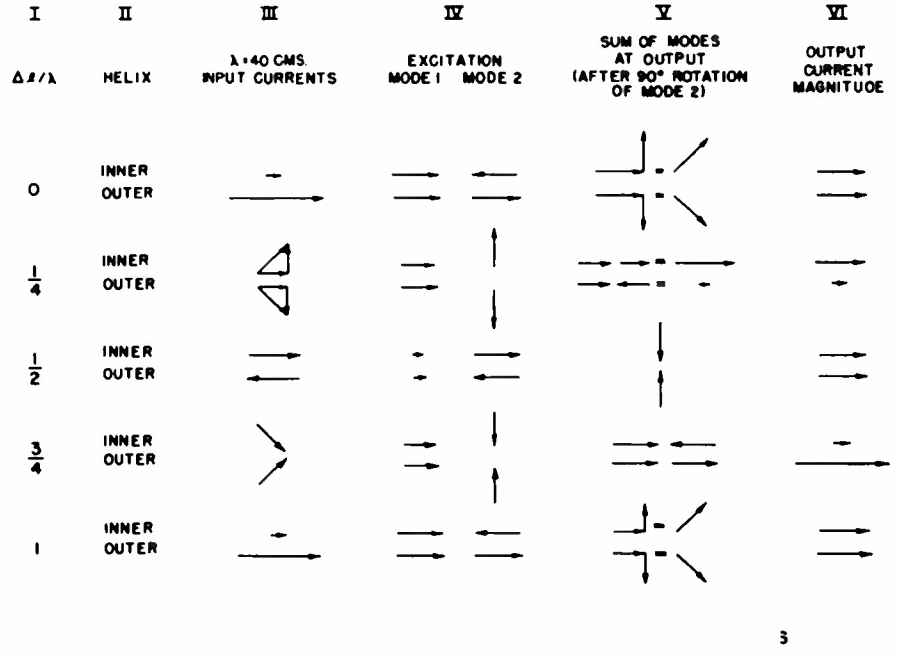

Fig. 21 Diagram of current vectors in cross-wound double helices (phases measured relative to current phase in Mode 1).

of equal length the boundary conditions for matching the input currents can be met by establishing Mode 1 only. Figure 18 indicates that the apparent input impedance to the inner helix is very high for $\Delta\ell/\lambda = 0$; i.e., the net current flowing in the inner helix at the input end is very small. The fact that the two input lines are equal requires that whatever currents flow in the two helices must be in phase. This condition on the phase can be satisfied by an almost equal mixture of the two modes adding up to give high current in the outer helix and an almost zero in-phase current in the inner helix. With this assumption, the vector diagram of Fig. 21 agrees in detail with the interference and VSWR curves of Fig. 18.

In Figs. 20 and 21, Column I identifies the relative shift in line length to the two inputs; Column II identifies the two helices; Column III shows the current excitation with the proper phase to agree with Column I; Column IV shows the relative excitation of the current vectors in the two fundamental modes to agree with Column III; Column V shows the vector sum of the two modes at the output and after Mode 2 has rotated 90° with respect to Mode 1; and finally, Column VI shows the expected magnitude of the output currents in the two helices as a result of the interference of Modes 1 and 2.

The qualitative agreement of Figs. 17 through 21 demonstrates again the existence of the two fundamental modes, one mode having in-phase currents and the other out-of-phase currents in the two helices. It is concluded that Mode 1 can be excited by connecting the two helices to separate lines of equal electrical length, perhaps tapering each line from, say, 100 ohms at the tee to the helix impedance for good matching. It is also seen that, to avoid exciting Mode 2 at the frequencies for which the structure is resonant in Mode 2, care must be taken to reduce sufficiently the Q of the circuit in Mode 2. The attenuator required to stabilize the tube in Mode 1 probably would be sufficient to damp the Mode 2 resonance, since the impedances and field configurations external to the annular gap are comparable in magnitude in the two modes.

C. Unidirectional Attenuators - S. E. Webber

Use is made of the fact that the electromagnetic field of a helix is elliptically polarized and that the resonance absorption of ferrite in such a field will cause an attenuation, the magnitude of which is dependent upon the direction of propagation of the wave.

Attenuation measurements were made on a cylinder of ferrite 2 cm long and closely surrounding the helix; curves of attenuation versus frequency

for constant exciting field are shown in Fig. 22. Investigation of the magnetic focusing field inside the sample indicated distortion due to the finite permeability of the ferrite. To reduce the effect, the cylinders were split into rings of length equal to thickness (about 1/8 inch long and 1/2 inch mean diameter). With about 1/8 inch air gap, the directional attenuation was measured again and found to be about the same as before. Although the exciting field was much higher, the distortion of the magnetic focusing field was reduced considerably, as would be expected.

An analysis of the electromagnetic fields outside of a sheath helix in free space gave the following ratios of magnetic components of the electromagnetic fields:

$$\frac{H_\phi}{H_r} = -j \frac{(\rho_0 a) \cot \psi}{(\rho a)(\gamma a)} \frac{K_1(\gamma a)}{K_0(\gamma a)}$$

$$\frac{H_z}{H_r} = +j \frac{\gamma a}{\rho a} \frac{K_0(\gamma r)}{K_1(\gamma r)}$$

The quantities H_ϕ and H_z are not out of time phase and are not considered.

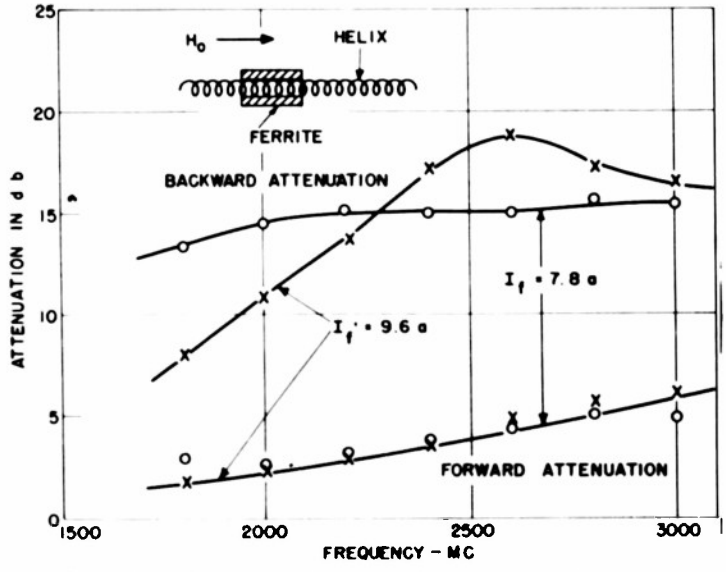

Fig. 22 Attenuation vs frequency for constant magnetic field.

The magnitude of this ratio gives the ratio of major to minor axis of the ellipse of polarization. It is seen that the magnetic vectors in the planes indicated are elliptically polarized (components are out of time phase), and in the case of the r-z plane the magnitude can be close to unity for large γa. From this it was deduced that a d-c interaction with magnetic field in the Φ direction in the ferrite should have a much more directional attenuation than that with an axial field. Thus far, efforts to find this resonance have been unsuccessful.

Inspection of the ellipticity in the $r - \Phi$ plane for large γ suggests a ratio about equal to $\tan \psi$, which is of the order of 0.1. The absorption effect measured with the axial magnetic field shows directional results much better than indicated by the simple analysis.

The ferrite itself, when immersed in a magnetic field, has a tensor permeability. An accurate and complete analysis of these fields is not easy. However, assuming an isotropic permeability μ outside the helix to infinity alters the above ratios in the following fashion:

$$\frac{H_\Phi}{H_r} = -j\mu \frac{(\beta_o a)\cot\psi}{(\beta a)(\gamma_2 a)} \frac{K_1(\gamma_2 a)}{K_o(\gamma_2 a)} ,$$

$$\frac{H_z}{H_r} = j \frac{\gamma_2 a}{\beta a} \frac{K_o(\gamma_2 r)}{K(\gamma_2 r)} ,$$

where γ_2 in Pierce's notation refers to the region of permeability μ outside the helix. The chief difference is that the ellipticity in the $r - \Phi$ plane can be made closer to unity by the permeability. This simple analysis gives some insight into the mechanism that makes the interaction with an axial magnetic field successful.

D. Electron Bunching in Traveling-wave Tubes - S. E. Webber

In Quarterly Progress Report 22, reference was made to preliminary measurements of the harmonic content of the electron beam of the traveling-wave tube by means of a collector consisting of a short gridded gap terminated by a 50-ohm coaxial line. This work has been continued. Also, preliminary tests have been conducted on a tube displaying the 400-Mc current pulse by a circular sweep on a fluorescent screen.

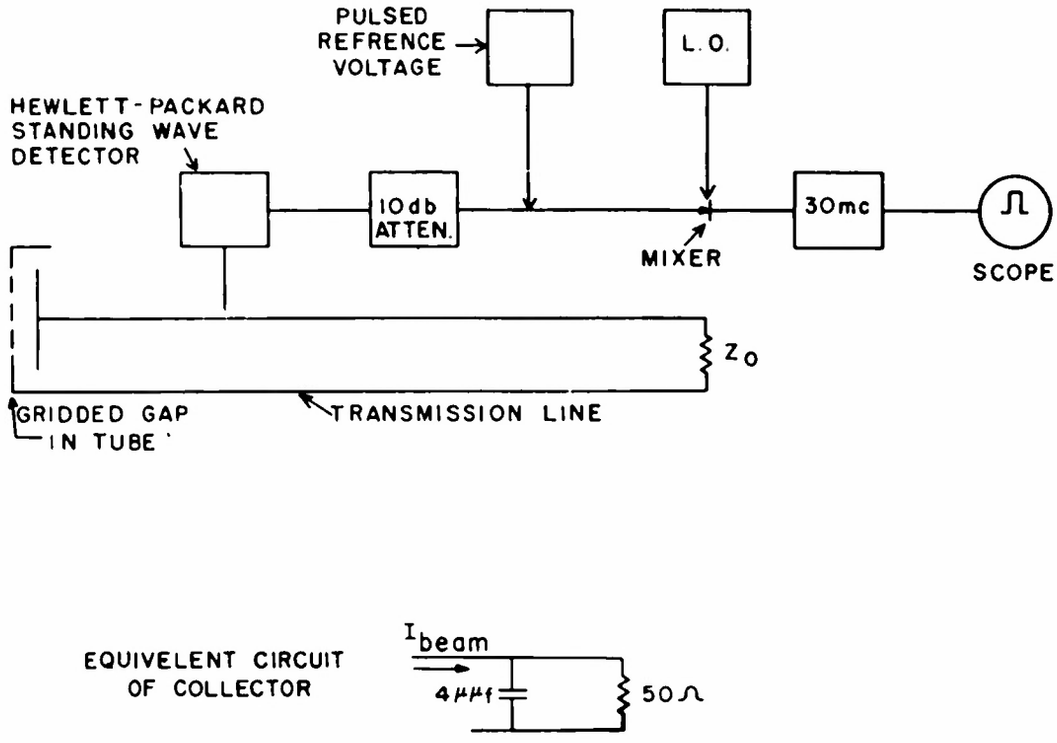

Fig. 23 Schematic of harmonic measuring system.

Considerable effort was expended in refining the technique for measuring the amplitude of harmonic signal in the coaxial line. The most suitable system is as follows (see Fig. 23). First, the traveling probe on the Hewlett-Packard slotted line was altered to provide a high-Q tunable resonant cavity. The most suitable detector was a local oscillator mixer and 30-Mc i-f amplifier system. This was necessary to provide sensitivity for some of the phase-comparison measurements that were made. Amplitude was measured by comparing the harmonic amplitude from the tube with the amplitude of the delayed pulse from a standard signal generator on the scope. The response of the over-all system to other harmonically related signals was checked, and all other responses were down by more than 30 db.

With suitable calibration, this system provides a measure of the amplitude of the harmonic voltage in the 50-ohm line directly in dbm. In order to refer this to beam current amplitude, an equivalent circuit is assumed for the collector. The beam current charges the capacitor

(in this case the capacitance of the gridded gap), and also a component flows in the 50-ohm resistor (in this case, the terminated 50-ohm line). With this circuit, amplitudes measured in the coaxial line can be referred to the corresponding amplitudes of beam currents.

At the gridded gap, certain electrons incident from the beam will be intercepted by the grid, and others in the form of secondary electrons will return to the grid after having traversed the gap. It is necessary to know how much of the current incident upon the collector is effective in inducing r-f current in the gap. This was investigated by applying a variable d-c voltage across the gap and noting the way the amplitude of the induced fundamental component varied with this voltage for a constant value of total beam current. It was observed that small amounts of bias voltage could change the d-c current to the center conductor and that the relationship between this current and harmonic amplitude was not linear until a very high accelerating voltage was applied. The pulse current flowing through the 50-ohm termination could provide enough bias voltage across the gap to cause an error in the harmonic beam current measurment. If the total voltage across the gap was zero when the pulse current was flowing, the resultant r-f current amplitude was in the same ratio to the average current to the center conductor as at very high gap voltage when there were no secondary electron effects. This condition of zero gap voltage was used to make measurements, and the rms amplitudes were increased by the ratio of average center conductor current to total collector current to refer the various harmonic amplitudes directly to beam current.

With the equipment operating as above, measurements were made of harmonic amplitude under various conditions. Figures 24 and 25 show typical curves of various harmonic amplitudes in the electron beam as a function of drive voltage. In one set, the beam voltage is adjusted for maximum small-signal gain, while in the other the beam voltage is adjusted for maximum power output. These show generally the peak value of fundamental component about 3 db below saturation power and the predominance in second-harmonic current in the beam at saturation. The first-, second-, and third-harmonic components are of the same order of magnitude near saturation. When the beam velocity is increased at saturation power, the second-harmonic component is reduced in amplitude while the fundamental is increased.

The ratio of rms amplitude of fundamental to d-c beam current I_{ac}/I_{dc} can be obtained from these measurments. While this has not been studied in detail, some preliminary results have indicated that this ratio is quite low. For instance, in the above data, the maximum ratio is

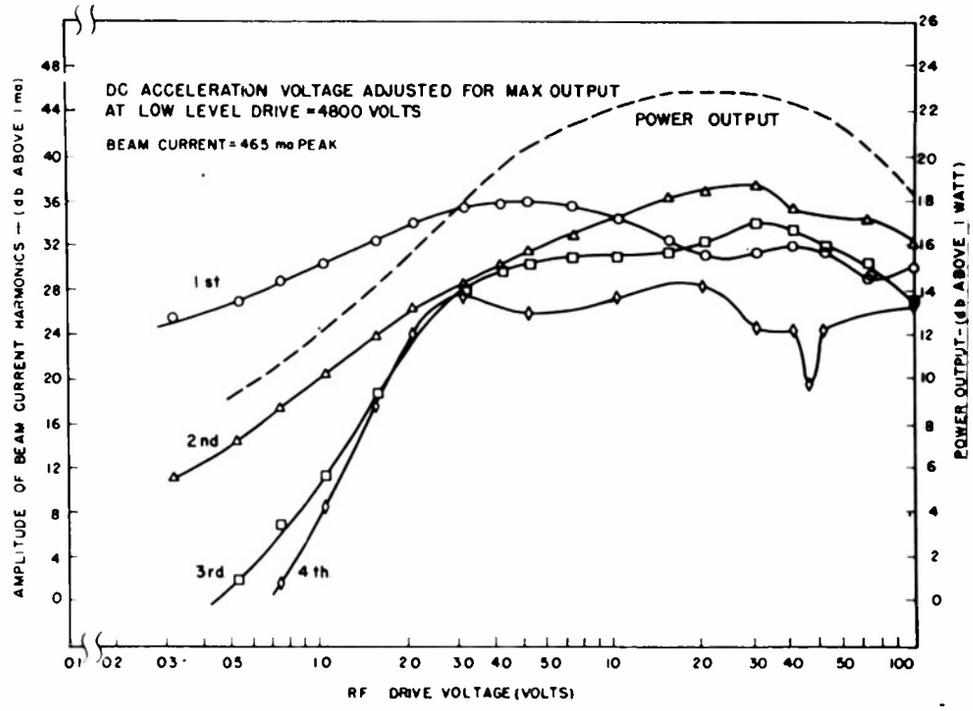

Fig. 24 Harmonic amplitudes and power output vs r-f drive.

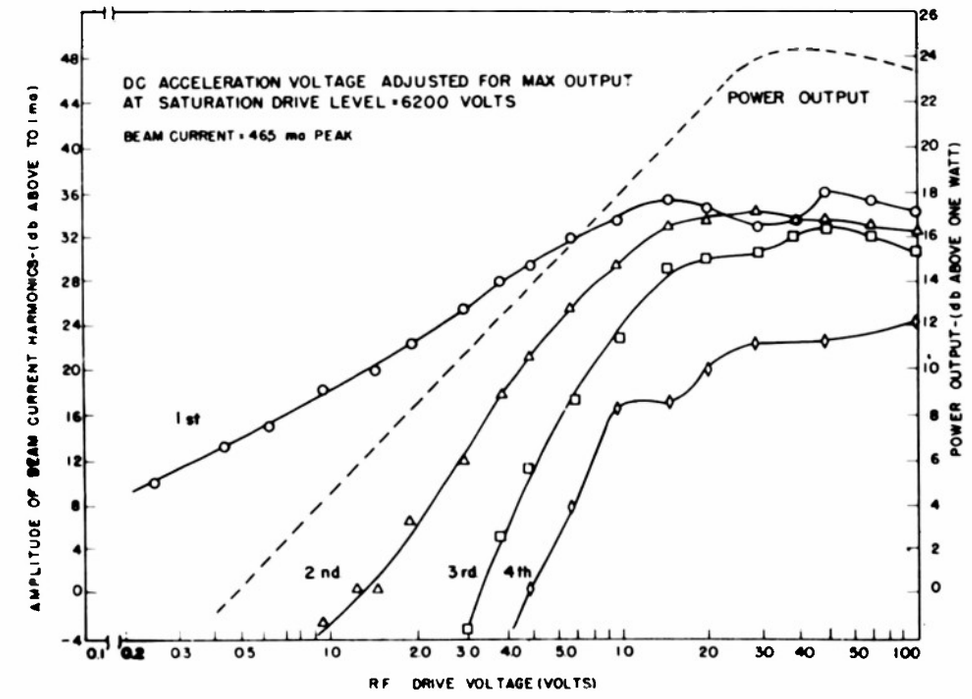

Fig. 25 Harmonic amplitudes and power output vs r-f drive.

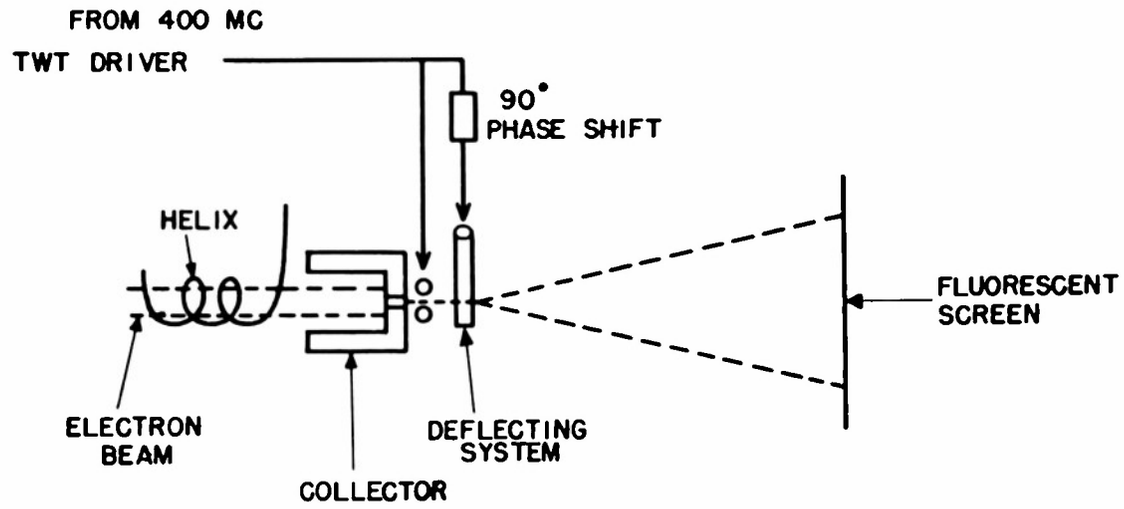

Fig. 26

about 0.14. The tube efficiency was about 15 per cent. Results so far suggest that this ratio decreases as beam current increases.

Another collector for this tube is shown schematically in Fig. 26. A small part of the electron beam passes through a pair of deflecting plates driven by a 400-Mc voltage and 90° in time phase. The beam appears on the fluorescent screen as a circle representing the 360° of the r-f cycle. On the screen, the intensity is a measure of density of current in the r-f cycle, and radial position indicates electron velocity. Slowed-down electrons are on the outside of the original circle. In the operation of the tube, the magnetic focusing field is a source of considerable difficulty in obtaining a good clean spot. Under certain circumstances, a picture can be obtained which seems to be representative of the r-f pulse of current in the electron stream. Figure 27 shows pictures taken of the circular sweep at points just below and just above saturation power. One observes a region of high density at "9 o'clock," consisting of electrons of two discrete energy levels. In approaching saturation, this density part is seen to rotate about 30° counterclockwise as the bunch is slowed down. Slower electrons appear to predominate at the lagging edge of the bunch. Past saturation, the density bunch is spread out in time, with new bunches of current appearing in different parts of the r-f cycle.

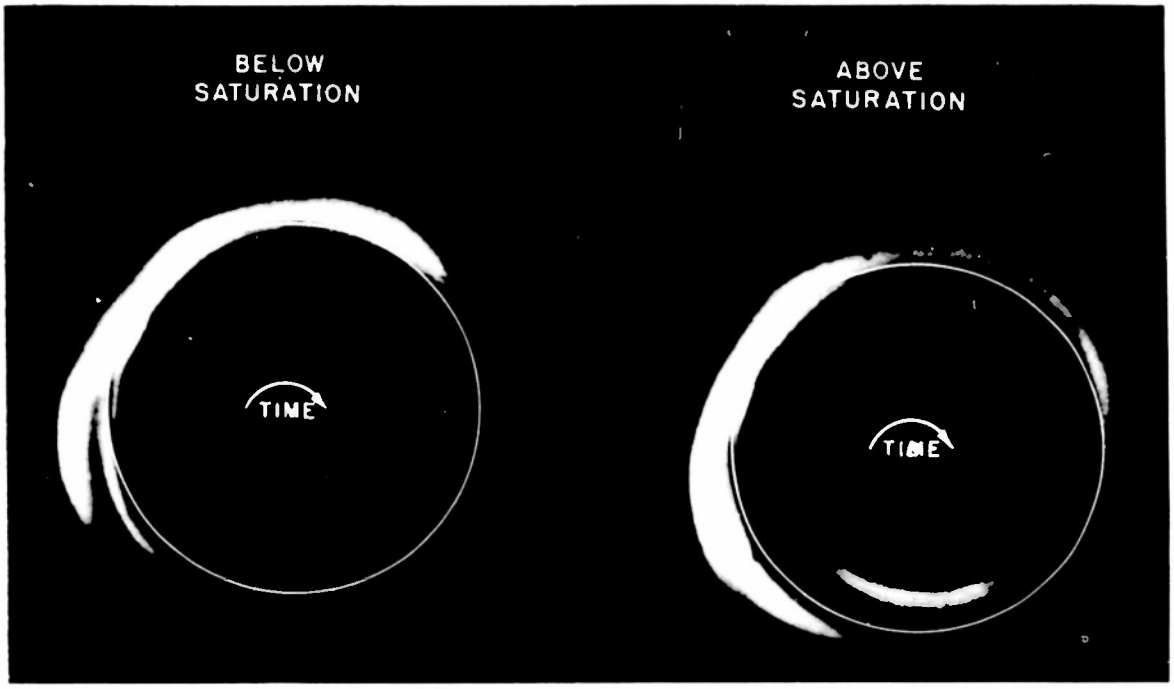

Fig. 27 R-f current pulse near saturation.

An improved version of this latter tube is being constructed. It is expected that this will have better focusing and colimating to eliminate unwanted effects due to the magnetic focusing field.

E. Resonant Spiral Circuits - J. A. Rich

In the previous report it was shown how a resonant helix could be coupled to a tunable resonant cavity. It was shown that, if one combined a helix section with a coaxial cavity resonator in such a way that the inner conductor of the coaxial resonator shielded the helix, except for a small gap near the end of the helix, coupling across the gap would be obtained. As a result of this coupling, one is able to "tune" the helix by changing the length of the coaxial cavity resonator.

In the present period of activity, work on the coupling of the two resonators has been continued, particularly along the following lines:

1. An improvement in the coupling (tunability of the resonant helix) has been obtained by terminating the inner conductor of

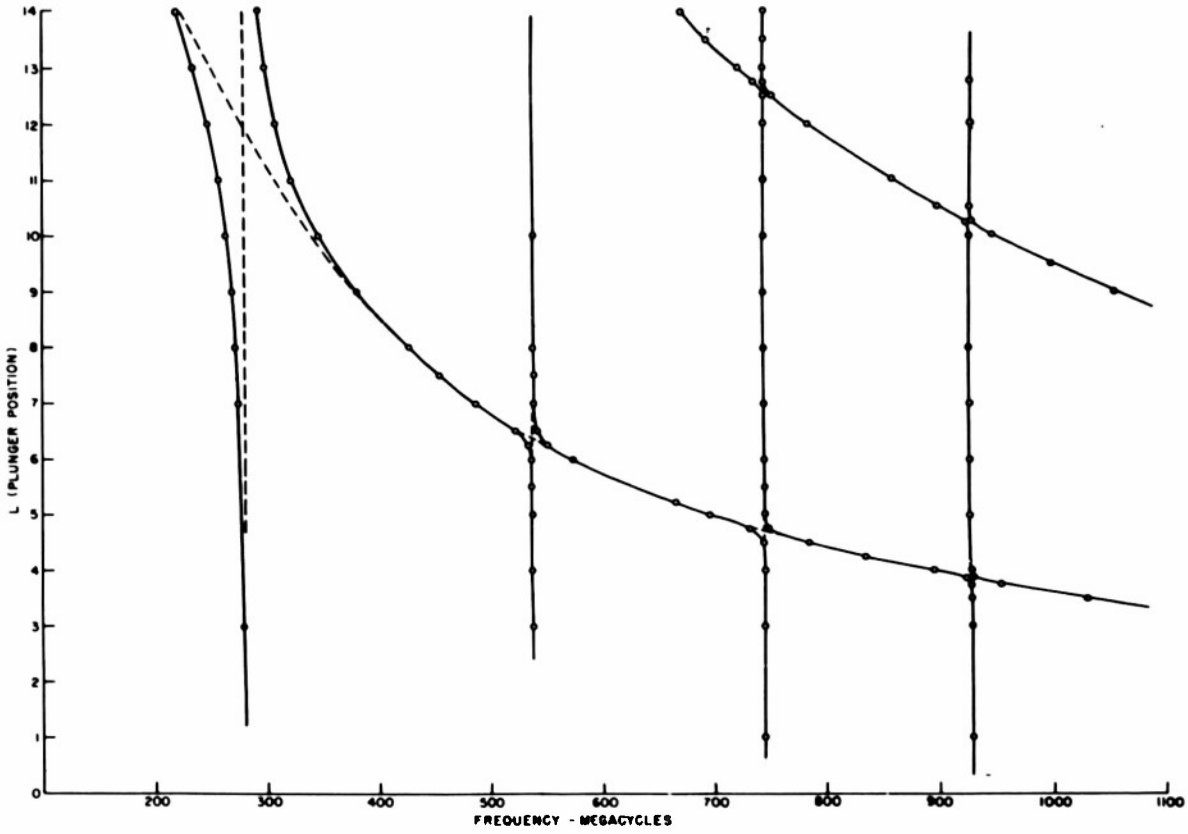

Fig. 28 Mode curves for helix-resonant cavity system. Gap spacing, δ = 3.5 cm.

the coaxial resonator in a hemispherical shell through which the helix projects. This allows the electric field across the gap to be brought in closer to the helix without losing helix impedance. The results obtained with this tighter coupling are shown in Figs. 28 and 29. In the first figure, the system tuning curve is shown for a gap spacing of 3.5 cm. This is the case of weak coupling. In Fig. 29, the system tuning curve is shown for a gap spacing of 1 cm, the case of optimum coupling.

2. The variation in the coupling of the two resonators as a function of gap spacing has been studied. The problem here was to determine the gap spacing associated with the optimum coupling. The coupling constant as a function of gap spacing is shown in Fig. 30 for the case of the inner conductor

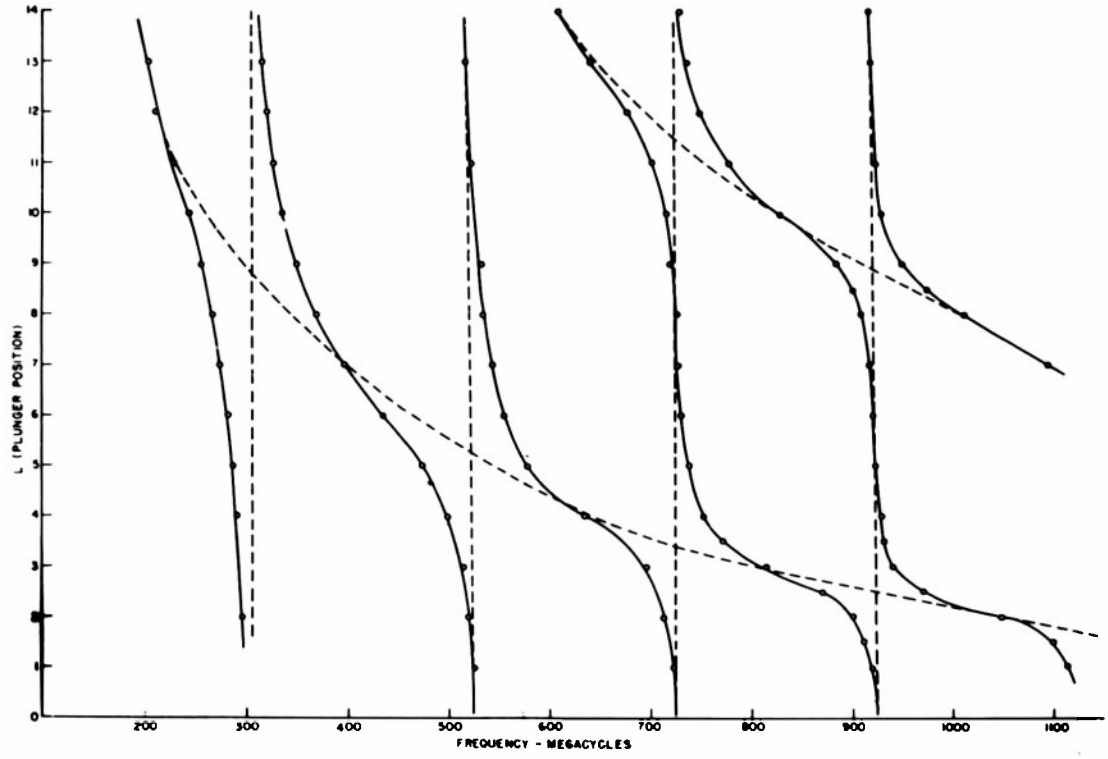

Fig. 29 Mode curves for helix-resonant cavity system. Gap spacing, 1 cm.

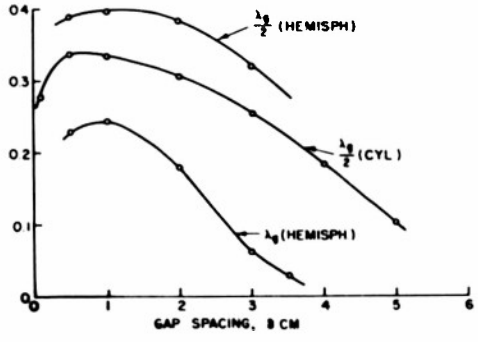

Fig. 30 Coupling constant vs gap spacing; helix-resonant cavity system.

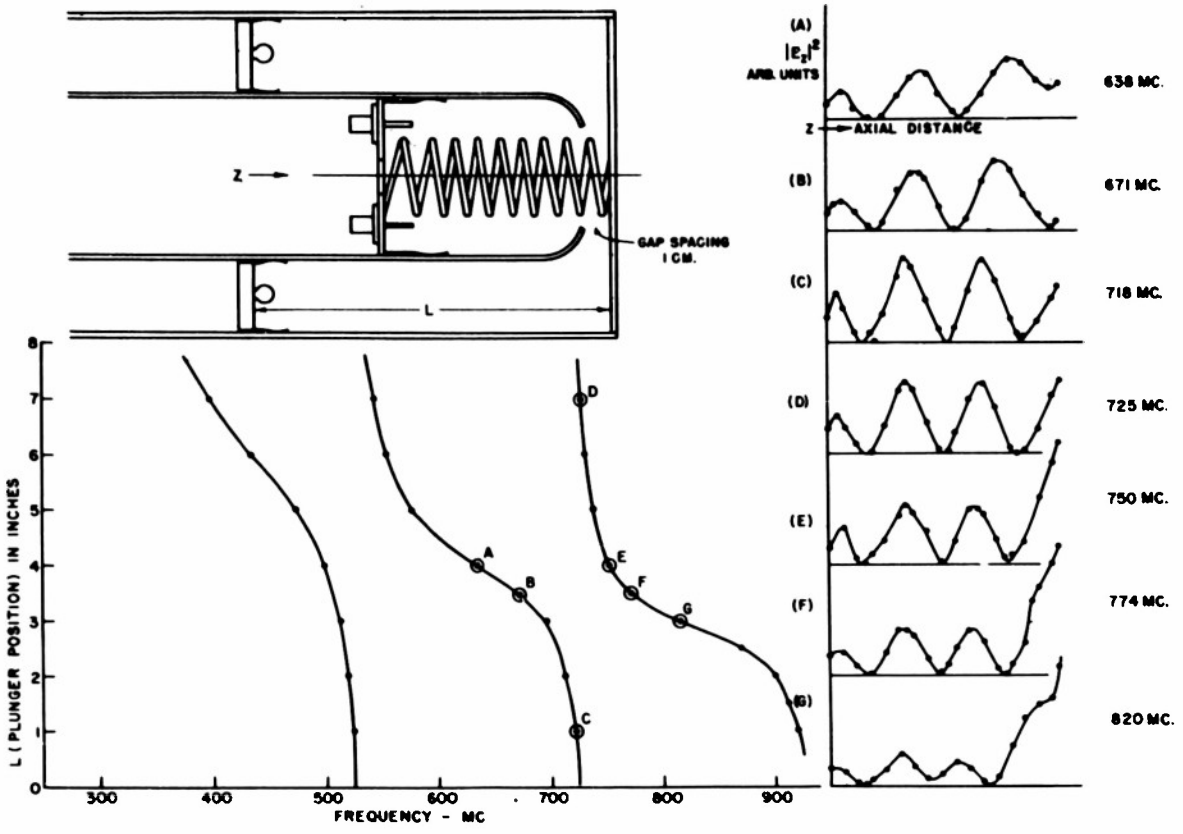

Fig. 31 Axial field distribution for helix-resonant cavity system.

terminated in a hemispherical shell through which the helix projects (see Fig. 31), and for the case in which the diameter of the inner conductor remains constant throughout its length. The ratio of diameters for the outer cavity cylinder, the inner conductor, and the helix was chosen to have the value 4 : 2 : 1.

3. The axial field distribution $|E_Z|^2$ has been determined as a function of frequency on the system tuning curves shown in Fig. 29. The region around the $3/2\,\lambda g$ mode for the helix was taken as being of particular interest. The quantity $|E_Z|^2$, which is plotted in arbitrary units in Fig. 31, is proportional to the shift in resonance frequency, $\Delta\nu$, obtained when the system is perturbed by a small sphere of TiO_2 placed at some point Z on the helix axis. It should be pointed out that $|E_Z|^2$ does not reach a maximum at Z = 0 comparable to the other maxima in the

field pattern, owing to the hole cut into the end plate to provide access for the dielectric sphere.

As an aid to interpreting the axial field distribution curves, it can be mentioned that Points C and D correspond to energy storage in the helix. As one moves to either side of the frequency corresponding to the $3/2\lambda g$ helix mode, one would expect less storage of energy in the helix and more storage of energy in the cavity. One would expect that at the inflection points A and G most of the energy would be stored in the cavity. That there are appreciable helix fields at these frequencies comes as a pleasant surprise.